# Quick Large-Area Detection of Thin Silicone Films with Coherent Raman Scattering Imaging

*Julian Naser,\* George Sarau, Jan Wrege, Michael Schmidt, and Silke Christiansen*

Coherent Raman Scattering Imaging offers quick and surface-sensitive large-area scans of specimens including fingerprinting of the substances, combined with low detection limits. By using a multi-photon process, it offers orders of magnitude stronger surface signal in comparison to spontaneous Raman (SR) and fluorescence signals of the substrate are avoided by the detection principle and the near-infrared laser wavelength. By exciting at a specific wavelength instead of measuring whole spectra the measurement time is remarkably reduced. Here, detecting organic thin films on glass surfaces is investigated. The detection of those thin films is relevant for production processes where the interfacial layer is influenced by the low surface energy of contaminants, especially polysiloxanes. The samples are manufactured by pipetting diluted polydimethylsiloxane (PDMS) in heptane in various concentrations (1%, 0.1%, 0.01%, and 0.001%) on glass substrates. After evaporation of the solvent, thin films of the silicone remain. The resulting average coverage of the thin films equals $100–0.1 \, \mu g \, cm^{-2}$. Measurements determine the detectability threshold with SR to $10 \, \mu g \, cm^{-2}$, while the acquired spectrum is used to determine characteristic peaks for the pump laser. Afterwards the samples are imaged at those wavenumbers with Coherent Raman Scattering (CRS) Imaging techniques providing a chemically-specific contrast.

## 1. Introduction

Organic thin film contaminations are a common problem in production processes like adhesive bonding, coating, and lithography where the interfacial layer is crucial. The low surface energy of contaminants like polydimethylsiloxane (PDMS),

can weaken the bonding and lead to failures.[1–6] To avoid those issues various techniques like X-ray photoelectron spectroscopy (XPS), contact angle measurement, scanning electron microscopy (SEM) combined with energy-dispersive X-ray spectroscopy (EDX), and spontaneous Raman (SR) can be used to detect thin films, yet the effort for those analytics including sample preparation, vacuum conditions needed, measurement duration, degradation of the sample, and the limited sensitivity exceeds the benefits.[7–10]

This results in the need for a quick, contactless, surface sensitive, large-area measurement technique that doesn't require sample preparation or vacuum conditions. From the techniques compared in **Table 1**, SR was picked as the most promising technique with the only shortcomings being the long duration of the measurements and the medium sensitivity. Its acquisition of a complete spectrum is suitable to detect and identify unexpected types of contaminations and to determine characteristic peaks. For the targeted analysis of samples those characteristic peaks are used for coherent Raman scattering imaging techniques that enhance the sensitivity. In this article the multi-photon techniques simulated Raman scattering (SRS) and coherent anti-Stokes Raman scattering (CARS) have been investigated. Theoretically the detection of thin films down to one atomic layer on water surfaces is possible

J. Naser, J. Wrege
Siemens Healthineers AG
Siemensstraße 1, 91301 Forchheim, Germany
E-mail: julian.naser@fau.de

J. Naser, M. Schmidt
Institute of Photonic Technologies
Friedrich-Alexander-Universität Erlangen-Nürnberg
Konrad-Zuse-Straße 3/5, 91052 Erlangen, Germany

The ORCID identification number(s) for the author(s) of this article can be found under https://doi.org/10.1002/pssa.202300750.

J. Naser, G. Sarau, S. Christiansen
Institute for Nanotechnology and Correlative Microscopy eV (INAM)
Äußere Nürnberger Str. 62, 91301 Forchheim, Germany

G. Sarau, S. Christiansen
Fraunhofer Institute for Ceramic Technologies and Systems (IKTS)
Äußere Nürnberger Str. 62, 91301 Forchheim, Germany

G. Sarau
Max Planck Institute for the Science of Light
Staudtstraße 2, 91058 Erlangen, Germany

M. Schmidt
School of Advanced Optical Technologies
Friedrich-Alexander-Universität Erlangen-Nürnberg
Paul-Gordan-Straße 6, 51052 Erlangen, Germany

S. Christiansen
Physics Department
Freie Universität Berlin
Arnimallee 14, 14195 Berlin, Germany

**Table 1.** Comparison of measurement techniques for thin film detection.

| Technique | Sample preparation needed | Vacuum condition needed | Duration of measurement | Contactless | Spatial resolution | Sensitivity |
|---|---|---|---|---|---|---|
| Contact Angle | No | No | High | No | Low [mm] | High |
| SEM + EDX | Yes | Yes | High | Yes | High [nm] | High |
| Spontaneous Raman | No | No | High | Yes | Medium [μm] | Medium |
| XPS | Yes | Yes | High | Yes | High [nm] | High |

with CARS.[11] Practically this article investigates the detectability of thin films down to $0.1\,\mu g\,cm^{-2}$ with CRS. Therefore, SR, SRS, and CARS have been compared on various thin films. **Figure 1**a illustrates the setup used to investigate the transparent samples with the PDMS contamination on the lower surface. The red arrow symbolizes the excitation path of the pump-laser and for SRS and CARS also the Stokes-laser. The green one stands for the detection path of those Raman scattered photons after the interaction with the PDMS molecules. In the case of SR, it mainly includes the elastically scattered photons, but also a tiny fraction of less than one in a million of the incident photons, which are inelastically scattered by a molecular bond vibration that leads to red-shifted Stokes-photons. In the case of coherent Raman scattering imaging techniques, SRS and CARS, red-shifted Stokes-photons and blue-shifted anti-Stokes photons are emitted, respectively. Thus, with these spectroscopic investigations the characteristic change of energy of the red- or blue-shifted photons are measured. The Jablonski diagrams in Figure 1b–d show the main difference between SR and the CRS techniques, SRS and CARS: The usage of a second Stokes laser in addition to the monochromatic pump laser enables to excite specific vibrational modes of the contaminants in vibrational resonance, which multiplies the signal strength. At SRS the energy conversion between the two lasers is measured, while at CARS the blue-shifted anti-Stokes photons are counted. The advantage of CARS is the avoidance of the fluorescence that takes place in the red-shifted part, since in the measured, blue-shifted part no fluorescence is contained. Instead, an inherent non-resonant background is measurable, especially when measured in transmittance.[12–14]

For this investigation CARS is appealing, because in comparison to SRS the required instrumentation is less complex, which is advantageous for inline check of parts in a production line. Vibrational spectroscopy such as SR, Fourier-transform infrared
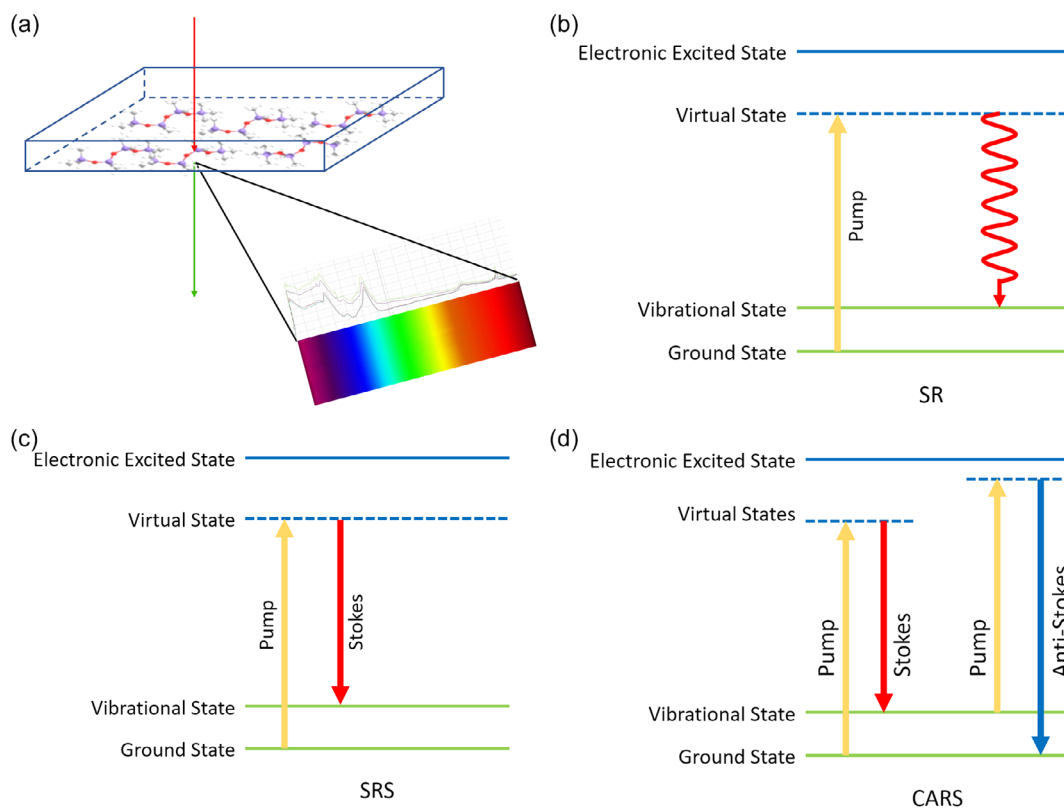


**Figure 1.** a) Overview of the measurement geometry for transparent samples. b–d) Jablonski diagrams explaining the SR, SRS, CARS effects used to detect thin silicone films on glass substrates.[22]

spectroscopy (FTIR) and near-infrared spectroscopy is already in use in the pharmaceutical industry to control the product quality without process interruption, although the article mentions that the weak Raman signal and possible interferences reduces the reliability of those measurements.[15,16] Furthermore the detection of PDMS in human tissue with SRS has been investigated by van Haasterecht et al.[17]

## 2. Experimental Section

### 2.1. Sample Preparation

The glass samples with the PDMS thin films on top were manufactured from standardized microscopy slides according to ISO 8037/1 and a dilution made from n-Heptane >99% and Siluron 5000. 10 µL of this dilution were pipetted on the glass surface and formed a droplet with an area of 1 cm², which equals a diameter of 1.128 cm. After evaporation of the Heptane, thin silicone films with various thicknesses remain. The coffee ring effect leads to higher film thicknesses at the perimeter of the pipetted droplet because of the capillary flow.[18,19]

With the density of 0.97 g cm⁻³, the covered area, the volume, and the percentage of the dilution, assumptions about the average film thickness can be made. **Table 2** shows the results of those calculations. The 1 percent dilution equals an average coverage of 100 µg silicone per cm² and 1 µm film thickness with big deviations. To ensure that the film thickness at the measurement point is equal or below the calculated average layer thickness, the perimeter of the contamination is just used to roughly focus the measurement system and the measurements are conducted at the center of the contamination. This approach underestimates the capabilities of the method and by that enables to predict if thin films with a certain thickness are detectable.

### 2.2. Characterization Methods

The samples were characterized for SR with a Nd:YAG laser (532 nm) using the Horiba LabRAM Explora Raman Spectrometer with the Syncerity OE detector and the Instrument Response Correction on. The laser power was 15.275 mW, the lens objective was the Olympus 50X LWD with a spot size of 1.3 µm, the grating used was 300 lines/mm, the measurement time was 225 s (15 s with 15 accumulations), the step size of the spectral scans was 2.04 cm⁻¹, the spectrum was taken from −50 to 3200 cm⁻¹.

**Table 2.** Concentration of the solution and the calculated resulting average coverage with silicone.

| Concentration [%] | Average film thickness [nm] | Average surface coverage [µg cm⁻²] |
|---|---|---|
| 10 | 10 000 | 1 000 |
| 1 | 1 000 | 100 |
| 0.1 | 100 | 10 |
| 0.01 | 10 | 1 |
| 0.001 | 1 | 0.1 |

The SRS and CARS measurements were performed with a Leica Stellaris SP8 CRS Coherent Raman Scattering microscope with a CARS 2000S filter and a HC PL FLUOTAR 10×/0.30 objective that offers a working distance of 11 mm. The wavelength used to excite the surface was 1032 nm for the Stokes beam, while the Pump beam was tuned between 800.5–784.6 nm, corresponding to 3050–2800 cm⁻¹. The measured area was 512 × 512 pixels at a pixel size of 2.275 µm, equal to an area of 1162.5 × 1162.5 µm, the scan speed was 400 Hz, the pixel dwell time equaled 3.1625 µs. The step size of the spectral scans was 15.91 cm⁻¹, the spectrum was acquired from 2800 to 3050 cm⁻¹.

## 3. Results and Discussion

**Figure 2**a shows the whole Raman spectra of different PDMS concentrations taken with the same measurement settings, while Figure 2b displays the characteristic wavenumbers in the range of 2800–3050 cm⁻¹. The peak at 2906 cm⁻¹ can be assigned to the symmetric stretching of the carbon-hydrogen bond and the peak at 2969 cm⁻¹ is a result of the asymmetric stretching of the carbon-hydrogen bond.[20]

The two peaks are clearly visible at the 100 and 10 µg cm⁻² concentration, at the 1 µg cm⁻² concentration the peaks are less distinct. The peaks at 2850 cm⁻¹ (symmetric stretching) and 2880 cm⁻¹ (antisymmetric stretching) derive from accidental contamination.

Consequently the thin film with an average layer thickness of 1 µg cm⁻² is the lowest detectable one. At the 0,1 µg cm⁻² surface coverage the two selected peaks are not visible at all, that means this thin film is clearly below the detection limit of SR spectroscopy.

To compare the detectability of the silicone contamination, the multi-photon techniques SRS and CARS are being used at the same samples. **Figure 3** shows a comparison of SR, SRS and CARS normalized to the degree of utilization of the detector for the two PDMS selected wavenumbers 2906 and 2969 cm⁻¹. The analysis of the measurements at 2906 cm⁻¹ shows that all concentrations were detectable with SRS as well as with CARS. The evaluation at the second wavenumber 2969 cm⁻¹ also shows that all concentrations were detectable, although the CARS signal at 2969 cm⁻¹ is weaker than the CARS signal at 2906 cm⁻¹. Regardless of the differences in the physical mechanisms of the methods, those results show the low detection limits and the high sensitivity of SRS and CARS.

Each SR measurement took 225 s for one pixel. The CARS and SRS measurements took 1 s each. In that time 262 144 pixels with a pixel size of 2.275 µm are measured. That equals 3.8 µs per pixel. The method with CARS or SRS is roughly 60 million times faster than SR. To measure the 1162.5 by 1162.5 µm area with SR a factor 100 reduced resolution, equivalent to a pixel size of 100 µm and 25 pixels on the area, would take 1.5 h of measurement time.

The CARS fingerprinting capabilities are visible in Figure 3c, the black ROI1 spectrum represents a region of interest covered with 10 µg cm⁻² of PDMS, the red ROI2 spectrum is measured on a clean area. The two peaks at 2906

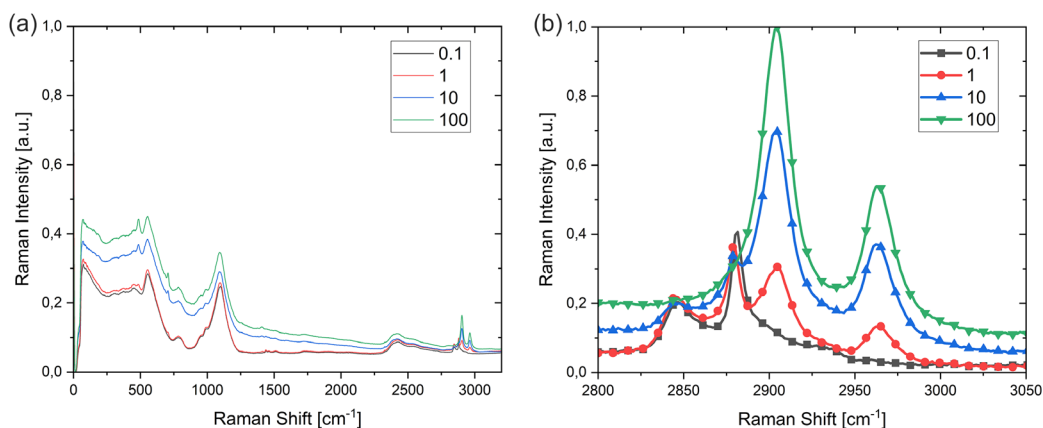**Figure 2.** a) Spontaneous Raman spectra for various surface coverages of PDMS in [μg cm$^{-2}$]. b) An excerpt of the 2800–3050 cm$^{-1}$ spectral range with specific PDMS peaks showing decreasing Raman intensity with lowering concentration.
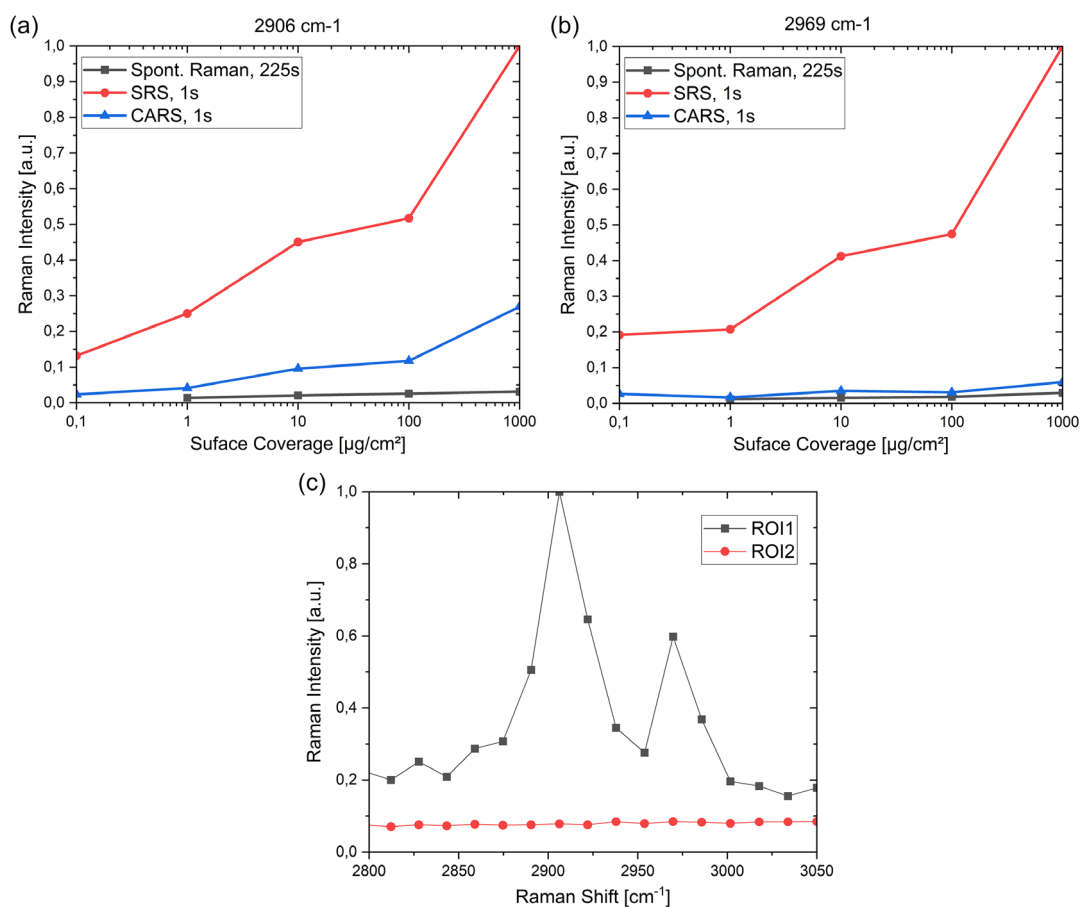


**Figure 3.** a,b) Comparison of signal strength for SRS, CARS, and SR at 2906 and 2969 cm$^{-1}$, normalized for laser power, detector sensitivity, detector gain, and baseline corrected. c) Example of a CARS spectrum for an area with 10 μg cm$^{-2}$ PDMS (ROI1) and clean glass area (ROI2).

and 2969 cm$^{-1}$ are clearly visible and thereby an identification of substances is possible.

**Figure 4** demonstrates the large-area scan (1 mm × 1 mm) capabilities of the SRS and CARS measurements at 1 μg cm$^{-2}$ concentration taken at the same spot on the edge area of a PDMS contaminated surface. The SRS image profits from the lack of non-resonant background.[21] The large-area scans were conducted with at the wavenumber 2906 cm$^{-1}$, which was selected based on the results shown in Figure 3.
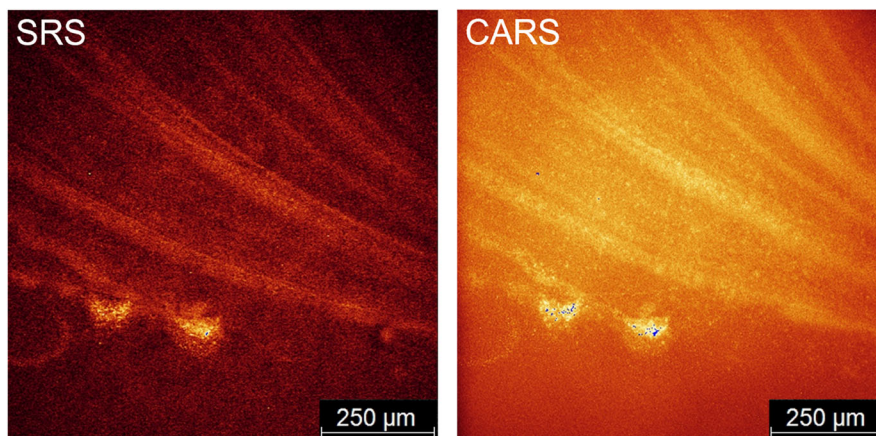
**Figure 4.** SRS and CARS imaging of PDMS contaminated glass surface with visible coffee ring effect acquired at 2906 cm$^{-1}$.

## 4. Conclusion

The results of the practical application of CRS imaging on the detection of PDMS thin films on glass substrates demonstrate the capabilities of those techniques. In this work the limits of detection of SR have been determined to 10 µg cm$^{-2}$ at a measurement time of 225 s per pixel. Those measurements have been repeated with CARS and SRS, there the thin films down to 0.1 µg cm$^{-2}$ were detectable with measurement times of 1 s for 262 144 pixels. This shows the lower detection limits as well as the time advantage. Because of the different detection principle and the use of near-infrared laser wavelength the signal from the substrate can be avoided. Further measurements showed the large-area scan capabilities. An area of 1 cm$^2$ can be scanned within minutes with a resolution of 2.275 µm per pixel. Furthermore, the opportunity for assigning the substance by the characteristic peaks was presented.

For future studies the investigation of the thin film detection on opaque surfaces in the epi reflection geometry and the quantification of the layer thickness will be addressed.

## Conflict of Interest

The authors declare no conflict of interest.

## Data Availability Statement

The data that support the findings of this study are available from the corresponding author upon reasonable request.

[1] C. S. Borges, E. A. Marques, R. J. Carbas, C. Ueffing, P. Weißgraeber, L. F. Da Silva, *Proc. Inst. Mech. Eng., Part C* **2021**, *235*, 527.

[2] D. N. Markatos, K. I. Tserpes, E. Rau, S. Markus, B. Ehrhart, S. P. Pantelakis, *Composites, Part B* **2013**, *45*, 556.

[3] G. L. Anderson, S. D. Stanley, G. L. Young, R. A. Brown, K. B. Evans, L. A. Wurth, *J. Adhes.* **2010**, *86*, 1159.

[4] D. M. Mattox, in *Surface Contamination* (Ed: K. L. Mittal), Springer, Boston, MA **1979**, https://doi.org/10.1007/978-1-4684-3506-1_15.

[5] R. Ledesma, F. Palmieri, B. Campbell, W. Yost, J. Fitz-Gerald, G. Dillingham, J. Connell, *Appl. Spectrosc.* **2019**, *73*, 229.

[6] M. P. Edward, *Met. Finish.* **2013**, *111*, 27.

[7] M. P. Seah, *Vacuum* **1984**, *34*, 463.

[8] J. F. Rabolt, R. Santo, J. D. Swalen, *Appl. Spectrosc.* **1980**, *34*, 517.

[9] D. Tsikritsis, E. J. Legge, N. A. Belsey, *Analyst* **2022**, *147*, 4642.

[10] P. Maillot, C. Martin, A. Planchais, *AIP Conf. Proc.* **2011**, *1395*, 227.

[11] J. Wang, G. Wloch, T. Lin, Z. Chen, *Langmuir* **2021**, *37*, 14540.

[12] M. Müller, A. Zumbusch, *ChemPhysChem* **2007**, *8*, 2156.

[13] C. Krafft, B. Dietzek, J. Popp, *Analyst* **2009**, *134*, 1046.

[14] J.-X. Cheng, W. Min, Y. Ozeki, D. Polli, *Stimulated Raman Scattering Microscopy*, Elsevier, Amsterdam **2022**.

[15] H. I. Kim, B. A. Morgan, J. P. Nokes, R. J. Zaldivar, *J. Adhes.* **2015**, *91*, 320.

[16] V. E. Andrew, G. K. Sergei, *Spectrochim. Acta, Part A* **2018**, *197*, 10.

[17] L. van Haasterecht, L. Zada, R. W. Schmidt, E. de Bakker, E. Barbé, H. A. Leslie, F. Ariese, *J. Biophotonics* **2020**, *13*, e201960197.

[18] M. Dileep, B. E. Huseyin, *Adv. Colloid Interface Sci.* **2018**, *252*, 38.

[19] Y. Mingwei, C. Dejian, H. Jie, Z. Xinyu, L. Zu-Jin, Z. Haomiao, *TrAC, Trends Anal. Chem.* **2022**, *157*, 116752.

[20] C. Dengke, N. Andreas, K. Rüdiger, H. Michael Heise, *J. Mol. Struct.* **2010**, *976*, 274.

[21] B. Manifold, D. Fu, *Annu. Rev. Anal. Chem.* **2022**, *15*, 269.

[22] B. R. Masters, P. T. C. So, *Handbook of Biomedical Nonlinear Optical Microscopy*, Oxford University Press, Oxford **2008**.